Chalcogenide Letters Vol. 20, No. 2, February 2023, p. 153 - 164

Preparation of CdS/g-C_3N_4 heterojunction photocatalyst with high activity sites by acid treatment

Y. L. Ma*, Y. Y. Tao
College of Physics and Electronic Information Engineering, Qinghai University for Nationalities, Xining 810007, China

The key to achieve efficient degradation of organic pollutants lies in improving the separation efficiency of photogenerated electron-hole pairs in photocatalysts. Here, the hydrogen bonds between g-C_3N_4 layers were broken by concentrated acid etching and exfoliation to obtain a more dispersed and lighter g-C_3N_4 nanosheet structure, and then the CdS spherical nanoparticles were dispersed on g-C_3N_4 nanosheets by hydrothermal method. The optimal loading of CdS on g-C_3N_4 nanosheets was determined by testing the degradation performance of the composite photocatalysts with different loading amounts. The degradation performance was tested by simulating sunlight using a 700-800 W xenon lamp equipped with a 420 nm cut-off filter, which showed that the degradation of MB by 7% CdS/g-C_3N_4 photocatalyst was 90.7% for MB. It indicates that concentrated acid treatment and loading of CdS nanoparticles can significantly improve the photocatalytic activity of g-C_3N_4 nanosheets, which is attributed to the enhancedup conversion function of g-C_3N_4 by loading CdS to enhance the response range and ability of g-C_3N_4 in visible light and the photogenerated electron-hole pair separation rate by loading CdS, thus improving the photocatalytic performance of the composite.

(Received November 16, 2022; Accepted February 15, 2023)
Keywords: CdS/g-C_3N_4, Photocatalytic, High activity sites

1. Introduction

Since the industrial revolution, traditional energy sources have been gradually depleted and the environment has been devastated. Therefore, the development of a new clean and renewable energy source has become an urgent task for mankind. The use of semiconductor photocatalysts for hydrogen production and degradation of organic pollutants has been found to be an effective means of solving many of the problems at hand[1].

These new energy sources have the advantages of a wide range of raw materials, high calorific value, with emphasis on no secondary pollution during use and mild conditions during preparation, such as TiO_2, ZnO, PdS, WO_3, g-C_3N_4, etc.[2,3]. However, many of the above types of photocatalysts suffer from a narrow visible light response range due to a wide band gap and thus cannot fully utilize sunlight, and photogenerated electron-hole pairs are highly susceptible to compounding, leading to their poor photocatalytic performance[4,5].Huang et al[6] prepared the Z-type photocatalyst $NiTiO_3$@ g-C_3N_4 by calcination, and in the prepared heterogeneous structure,

* Corresponding author: myl2005114@163.com
https://doi.org/10.15251/CL.2023.202.153

$NiTiO_3$ dispersed on the g-C_3N_4 surface can suppress the surface aggregation phenomenon of g-C_3N_4, which indirectly improves the photogenerated carrier separation efficiency of the sample, thus greatly improving the degradation rate of RhB and enhancing the photocatalytic activity of the sample. Peng et al[7] prepared a CdS@g-C_3N_4 N-N heterojunction photocatalyst, which can accelerate the electron transfer by the establishment of heterojunction and improve the separation efficiency of photogenerated electrons and holes, and thus substantially enhance the photocatalytic activity of the samples. Moreover, the establishment of heterojunctions also greatly enhances the stability of the samples. Many studies have demonstrated that either by elemental doping or heterojunction construction[8-10], these means can curb the frequent compounding of photogenerated carriers and greatly improve the photocatalytic activity of photocatalysts under visible light.

However, most of the reported photocatalysts for the degradation of organic pollutants have poor final physicochemical stability, low photogenerated carrier separation efficiency or cumbersome preparation process due to other phenomena such as surface agglomeration during the preparation process.

Here, g-C_3N_4 ultrathin nanosheet structures with high specific surface area were prepared by a simple method of concentrated acid etching and secondary calcination, and CdS nanoparticles with different mass ratios were loaded on this substrate material to select the composite photocatalysts with the highest photocatalytic activity under visible light. By characterizing the prepared photocatalysts and analyzing their degradation efficiency of organic pollutants under simulated visible light, we explain the reasons for the differences in photocatalytic performance and propose a reasonable photocatalytic reaction mechanism for the experimental results.

2. Experimental

2.1. Preparation of CdS/g-C_3N_4 composite photocatalyst

Firstly, 10 g of melamine powder was placed in a closed ceramic container and placed in a muffle furnace and heated at 550°C for 4 h. After the reaction was finished and cooled down naturally, the yellow lump of g-C_3N_4 was taken out and placed in a mortar, ground clockwise until the lump became a fine powder and then collected to obtain g-C_3N_4-1. 1g of g-C_3N_4-1 powder was taken in a beaker and 100 ml of deionized water was added immediately. After sonication, the g-C_3N_4-1 powder was collected by centrifugation and then dried in a drying oven at 60°C for 12 h. 1g of the dried g-C_3N_4-1 powder was taken in a beaker, 15 ml of 0.2 mol/L HNO_3 was added and the powder was sonicated for 2 h. After sonication, 150 ml of deionized water was added to dilute the original beaker. After the sonication, 150 ml of deionized water was added to dilute the liquid in the original beaker, and then the g-$C_3N_4(H^+)$ was collected by centrifugation and dried in a desiccator at 60°C for 12 h. The 400 mg of g-$C_3N_4(H^+)$ powder was placed in an open ceramic container and placed in a muffle furnace and heated under hot air at 500°C for 3 h. After the reaction was completed and cooled down naturally, the white g-C_3N_4 powder was removed and placed in a mortar and pestle. The white g-C_3N_4 powder was placed in a mortar, ground clockwise to a fine powder, and collected to obtain the g-C_3N_4-2 powder stripped by concentrated acid corrosion.

2.2. Synthesis of CdS/g-C_3N_4 nanocomposites:

CdS/g-C_3N_4 composite photocatalysts with mass ratios (CdS:g-C_3N_4) of 1%, 3%, 5%, 7% and 9%, respectively, were prepared by the ordinary hydrothermal method (taking 7% CdS/g-C_3N_4 loading as an example): Take 0.4009 g $CdSO_4$ powder and 0.0646 g $Na_2S_2O_3$ powder in a beaker, slowly add 30 ml deionized water, then slowly add 1 g acid corrosive g-$C_3N_4(H^+)$ powder under stirring, stir for 30 min, add 10 ml methanol dropwise and sonicate the reaction solution for 20 min, finally,the mixture was transferred into 100 ml Teflonlined stainless-steel autoclave an kept at 180℃ for 24 h. Finally transfer the mixed reaction solution to a tetrafluoroethylene lined After the system cooled down to room temperature naturally, the sample was collected by centrifugation and dried at 60°C for 12 h. The yellow mass was put into a mortar and ground clockwise for 30 min to obtain the yellow powder 7% CdS/g-C_3N_4.

2.3. Photocatalyst degradation performance test

The photocatalytic degradation performance was tested as follows: before light irradiation, a mixed suspension (35 ml) containing 35 mg of catalyst and 35 ml of 20 mg L^{-1} of the contaminant methylene blue (MB) was sonicated for 15 min and mixed well, then it was placed in a dark room for 30 min, after which 2-3 ml of the suspension was removed and the suspension was irradiated at 15°C using a 700-800 W xenon lamp equipped with a 420 nm cutoff filter. The suspensions were irradiated with a 700-800 W xenon lamp equipped with a 420 nm cut-off filter at 15°C, and the suspensions were taken at 10 min intervals, and finally the suspensions were centrifuged and the supernatant was collected.

2.3. Materials characterization

The samples were characterized by X-ray diffraction (XRD, D8 advanced, Bruker, Germany) with CuKα radiation (λ=1.5418 Å), scanning electron microscopy (SEM, S-4800, Hitachi, Japan), high-resolution transmission electron microscopy (HRTEM, Tecnai G2 F20, FEI, Netherlands). UV-Vis–NIR spectra at wavelength from 200 nm to 800 nm were collected with a UV-Vis–NIR spectrophotometer (UV-3600, Shimadzu, Japan). PL spectra were detected by a RF-5301PC Fluorescence spectrophotometer at room temperature using a 150-W Xenon lamp as the excitation source at the wavelength of 304 nm. X-ray photoelectron spectroscopy (XPS) was detected by a Thermo Fisher Scientific spectrometer(ESCALAB 250Xi). The BET specific surface area of samples was obtained from nitrogen adsorption–desorption data and measured using a surface area analyzer(Sibata SA-1100) at liquid nitrogen temperature. Electrochemical impedance spectroscopy (EIS) were investigated by a electrochemical station (CHI 660B). The light source used in this study was simulated solar light, emitted by a device equipped(HSX-F300) with a 300 W Xe lamp, which can output a stable continuous spectrum from ultraviolet to near infrared (300–2500 nm), similar to natural sunlight.

3. Results and discussion

3.1. Materials characterization

In order to understand the crystal structure of the composite nanomaterials, the prepared photocatalysts were characterized by XRD. As shown in Figure1, the diffraction peaks of both the

concentrated acid treatment and the loaded CdS nanoparticles are consistent with pure g-C_3N_4, and the characteristic diffraction peaks of CdS appear at 24.7°, 26.6°, 28.3°, 43.8°, 47.9° and 51.9° after the deposition of CdS on the g-C_3N_4 surface, corresponding to its crystallographic planes (100), (002), (101), (110) and (112), respectively, (002), (101), (110) and (112) crystal planes, respectively [18,19]. These results indicate that the composite of CdS and g-C_3N_4 was successful and that the crystal structure of the composite photocatalysts prepared by one-step hydrothermal method did not change more significantly due to the loading of CdS. In addition, it can also be seen from Fig.1 that the treated photocatalysts all have sharp and stronger diffraction peaks than pure g-C_3N_4, especially the 7% CdS/g-C_3N_4 composite photocatalyst, which indicates that the spectra start to become stronger with concentrated acid etching as well as CdS loading, a broadening of the visible response range, and an enhancement of the photocatalytic performance of the photocatalyst.

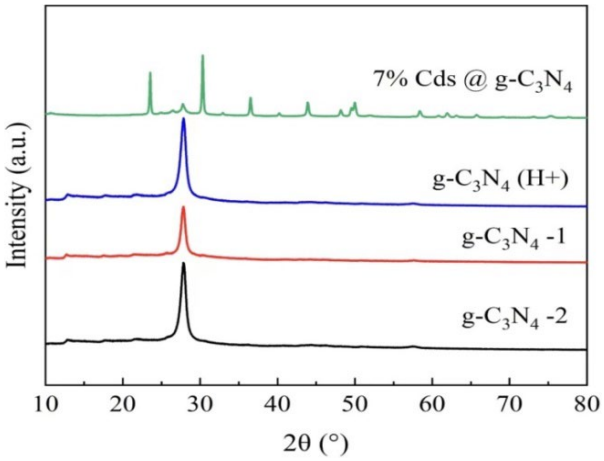

Fig. 1. XRD patterns of g-C_3N_4-1, g-C_3N_4-2, g-C_3N_4(H^+), 7%CdS/g-C_3N_4.

The SEM image of the prepared photocatalyst pure g-C_3N_4-1 is shown in Figure 2(a), from which it is easy to see that the pure g-C_3N_4 sample is a folded two-dimensional layered nanosheet structure, but due to the presence of hydrogen bonds between layers, it is highly susceptible to polymerization during heat treatment leading to a small specific surface area and fewer reactive sites, thus decreasing the photocatalytic activity. Therefore, g-C_3N_4(H^+) was obtained by using concentrated acid etching to break the hydrogen bonds between the layers of g-C_3N_4 nanosheets, as shown in Figure 2(b), which is slightly lighter and thinner compared with the nanosheets of g-C_3N_4-1 without acid treatment, but when it is further stripped by heat treatment, it can be found that, as shown in Figure 2(c), the g-C_3N_4-2 nanosheets Figure 2(d) shows the SEM image of 7% CdS/g-C_3N_4 composite photocatalyst, the CdS nanoparticles are more uniform and distributed on the g-C_3N_4-2 nanosheets after concentrated acid etching, and from Figure 2(e,f) also show that the substances with two different lattice stripe phases are affixed together. The crystalline spacing of 0.336 nm is the (002) crystalline plane of CdS, and the crystalline spacing of 0.325 nm corresponds to the (002) crystalline plane of g-C_3N_4 nanosheets [20,21]. both SEM and TEM results illustrate the successful composite of CdS/g-C_3N_4 materials and that a heterogeneous structure can be formed between these two substances, and the presence of the heterogeneous

structure can promote the photogenerated carrier separation efficiency and avoid compounding, which is essential to improve the photocatalytic performance of photocatalysts.

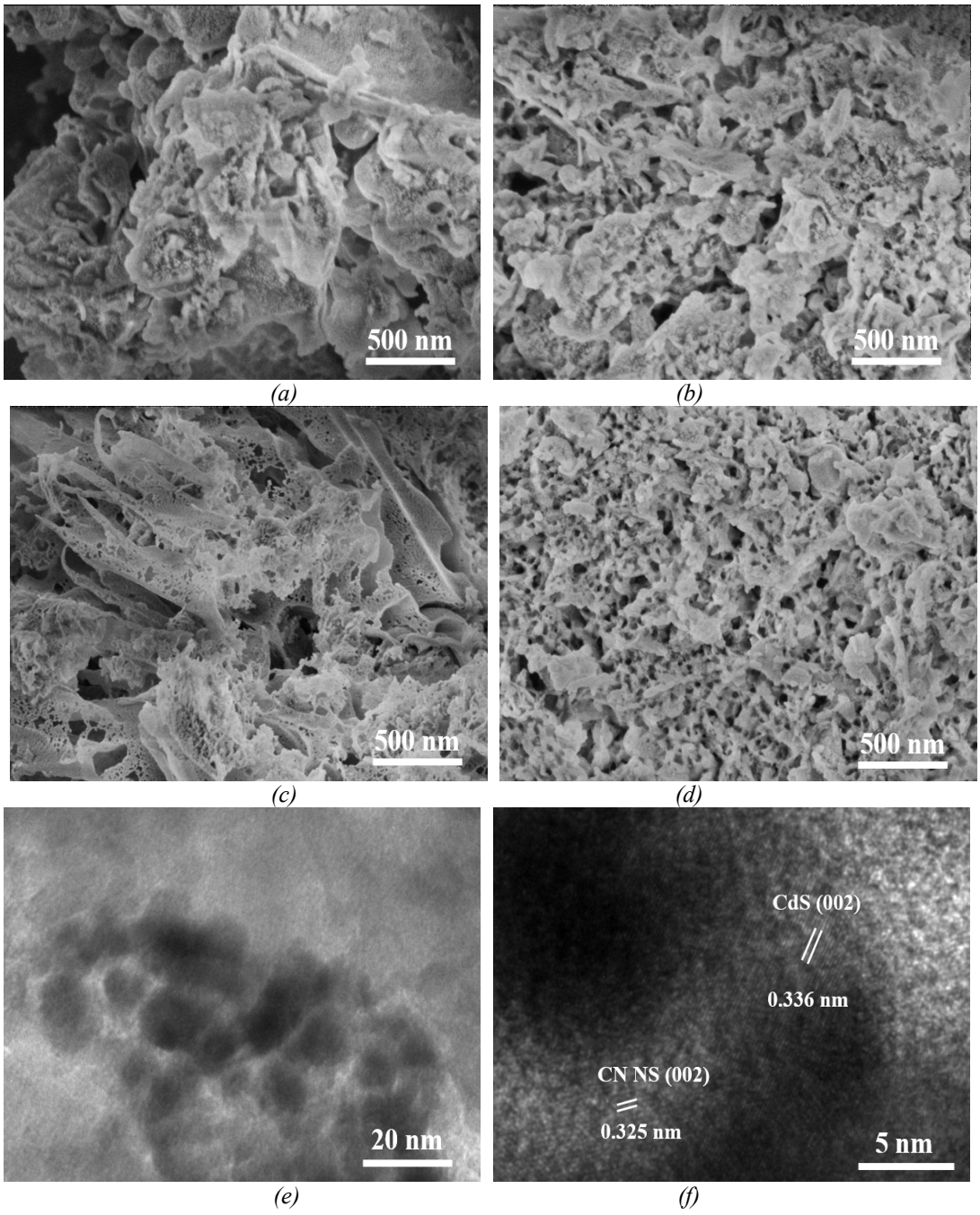

Fig. 2. SEM patterns of g-C_3N_4-1(a), g-$C_3N_4(H^+)$(b), g-C_3N_4-2 (c), 7% CdS/g-C_3N_4 (d) of photocatalysts and TEM patterns of 7% CdS/g-C_3N_4 (e,f) of photocatalysts.

The pore size distribution and specific surface area are an important indicator of the catalytic performance of photocatalysts, because usually, the larger the specific surface area, the more reactive sites are on the surface of the photocatalyst. Figure 3 and Table 1 show the nitrogen adsorption-desorption curves and the corresponding pore size distribution of the photocatalysts g-

C_3N_4-1, g-C_3N_4-2. It can be seen from the figures that the isotherm shapes of the two samples are similar before and after the acid modification, they both belong to type IV isotherm, and the pore diameters of both samples are between 0-50 nm, they both belong to mesoporous structure, and this mesoporous structure of photocatalyst generally has larger specific surface area and pore diameter[22], which is beneficial to the transport of photogenerated carriers inside the photocatalyst, thus improving the photocatalytic performance[23]. We can also clearly see that g-C_3N_4-2 modified by concentrated acid has a larger specific surface area, which is the theoretical basis for its stronger photocatalytic performance than that of g-C_3N_4-1.

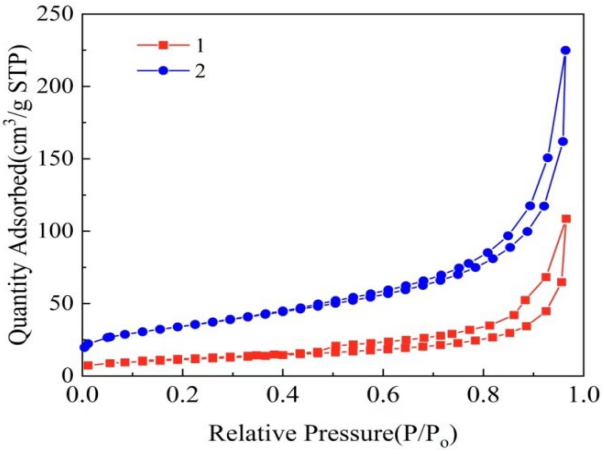

Fig. 3. N_2 adsorption/desorption isotherms of g-C_3N_4-1 and g-C_3N_4-2.

Table 1. BET surface area and Pore diameter of g-C_3N_4-1 and g-C_3N_4-2.

Sample	Specific surface area (m^2/g)	Pore diameter(nm)	Pore volume(cm^3/g)
g-C_3N_4-1	39.79	18.42	0.22
g-C_3N_4-2	121.65	21.98	0.56

Figure 4 shows the XPS spectra of the 7% CdS/g-C_3N_4 composite, and it can be seen from the general plot of Fig.4a that the composite photocatalyst contains C, N, Cd and N. This can also indicate the successful preparation of the CdS/g-C_3N_4 composite photocatalyst. From the high-resolution spectra of C1s (Figure 4(b)), it can be divided into two peaks of 284.8 and 288.2 eV, where the peak of 284.4 eV is attributed to the C-C bond and the peak located at 288.2 eV is due to the carbon bond reference peak of sp2 hybridization in the nitrogen-containing aromatic ring in g-C_3N_4[24]. From the high-resolution spectrum of N1s (Figure 4(c)), the peak with a binding energy of 399.7 eV corresponds to the sp^2-hybridized C-N=C bond in the triazine ring in g-C_3N_4. From the high-resolution spectra of Cd 3d (Figure 4(d)), it is known that the XPS peaks at binding energies of 404.9 eV and 411.6 eV are Cd $3d^{5/2}$ and $3d^{3/2}$, respectively[25].The peaks of S 2p at binding energies of 161.2 eV and 162.4 eV (Figure 4e) are attributed to S^{2-} in CdS[26] .The analysis of XPS patterns further proved the successful preparation of CdS/g-C_3N_4 composite photocatalyst.

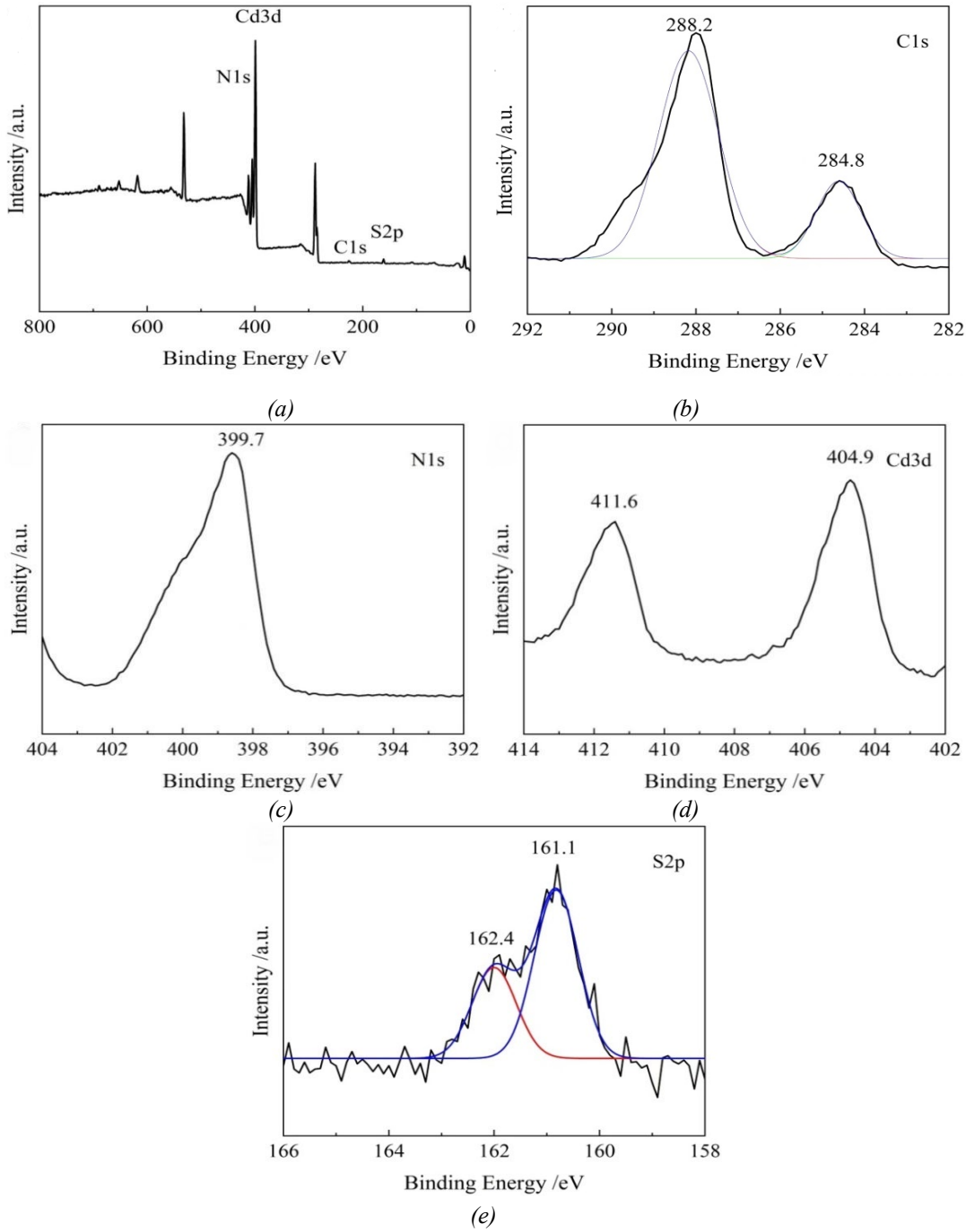

Fig. 4. XPS spectra of 7%CdS/g-C_3N_4 (a) and the corresponding high-resolution XPS spectra of C1s(b), N1s (c), Cd3d (d) and S2p (e).

In order to study the responsiveness and range of the prepared photocatalysts under UV-visible light, we used UV-visible diffuse reflectance spectroscopy scan for some of the prepared photocatalysts, because the magnitude of the photocatalyst response range to visible light severely limits the photocatalyst activity. It can be seen from the Fig.5 that the absorption edge of g-C_3N_4 is around 470 nm[27,28]. Both pure g-C_3N_4-1 and 7% CdS/g-C_3N_4 composite catalysts are able to respond to visible light. The g-C_3N_4-(H^+) underwent a weak red shift after concentrated acid

etching, but the 7% CdS/g-C_3N_4 composite photocatalyst red shift was more pronounced. This indicates that the successful composite of the two materials and contact to form a heterostructure narrowed the forbidden band width of the composite photocatalyst, which broadened the response capability and range of the photocatalyst in visible light, and facilitated the composite to absorb more light and generate more photogenerated carriers, which indirectly enhanced the photogenerated carrier separation efficiency, and also improved the up conversion function of pure g-C_3N_4 nanosheets, which greatly enhanced the photocatalytic activity of the photocatalyst.

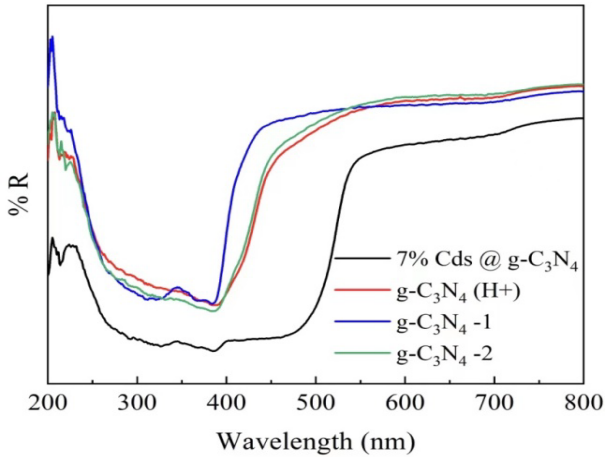

Fig. 5. Ultraviolet-visible diffuse reflectance absorption spectra of g-C_3N_4-1, g-C_3N_4-2, g-C_3N_4(H+) and 7%CdS/g-C_3N_4 photocatalysts.

3.2. PL and EIS spectroscopy characterization

PL spectroscopy is an important tool to measure the efficiency of the photogenerated electron-hole pair separation of the prepared samples, so we performed photoluminescence spectroscopy on the prepared photocatalysts. We know that when the sample is excited by certain light energy, the electrons inside the sample will jump from the valence band to its conduction band, leaving holes in the valence band, at which time a state of quasi-equilibrium will be formed, but the quasi-equilibrium is not very stable, and the electrons and holes they will compound again and emit light in the process, thus forming spectra with different energy distributions [29]. In other words, the stronger the spectral peak, the higher the rate of photogenerated electron-hole pair compounding; conversely, the weaker the spectral peak, then the higher the efficiency of photogenerated carrier separation and the stronger the photocatalytic activity possessed by the prepared material. As can be seen from Figure 6(a), the 7% CdS/g-C_3N_4 composite photocatalyst has the lowest value of fluorescence intensity, indicating that it has the highest photogenerated electron-hole pair separation efficiency, which is related to the formation of CdS/g-C_3N_4 heterostructure.

Figure 6(b) shows the electrochemical impedance profiles of the prepared photocatalysts, in order to further investigate the migration kinetics in the photocatalysts. Generally, the smaller the radius of curvature, the smaller the impedance available for charge transport and thus the better charge transfer characteristics, i.e., the smaller the radius of curvature, the more rapid the charge transfer within the material, the better the photogenerated electron-hole pair separation, and the

better the performance of the photocatalyst. It can be seen from the figure that 7% CdS/g-C_3N_4 composites have smaller radius of curvature than other photocatalysts, and thus have lower resistance to photogenerated electron migration, which is beneficial to the charge transport and separation within the system, and have stronger photocatalytic performance.

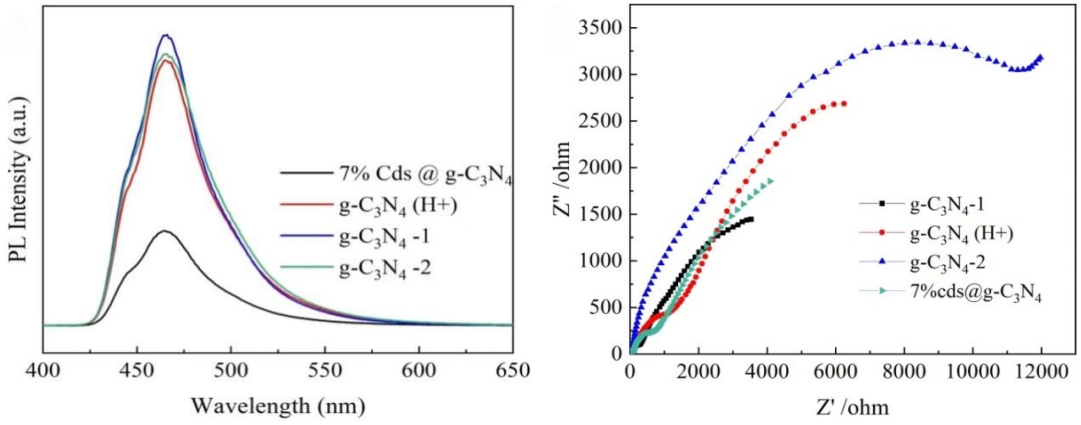

(a) *(b)*

Fig. 6. PL spectra (a) and EIS spectra(b) of photocatalysts.

3.3. Catalytic performance test

Figure 7(a) shows the effect of photocatalytic degradation efficiency test of the prepared photocatalyst for organic pollutant MB at a concentration of 20 mg L^{-1}. From the graph observation, it can be seen that the degradation rate of 7% CdS/g-C_3N_4 composite photocatalyst for MB (90.7%) is much higher and faster than that of g-C_3N_4-1(54.2%) under the same external conditions, Figure 7(b) shows the cycling degradation performance test graph of 7% CdS/g-C_3N_4 composite photocatalyst, and the sample can still reach a high degradation efficiency of 89.7% at the third cycle. In addition, we also tested the XRD patterns of the samples after the third cycle, as shown in Figure 7(c), and it can be seen that the XRD diffraction peaks of the samples did not change more obviously before and after the cycle, which indicates that the composite photocatalyst has a good physicochemical stability, which is firstly attributed to the concentrated acid corrosion modification of pure g-C_3N_4 (i.e. g-C_3N_4-1) itself, which increases its specific surface area and exposes more active sites. Secondly, probably due to the loading of CdS, the contact of the two substances formed a heterogeneous structure, which broadened the response capability and range of the composite photocatalyst in visible light, while promoting the migration rate of photogenerated carriers, allowing more pollutants to be degraded. In contrast, the degradation performance of the 9% CdS/g-C_3N_4 composite photocatalyst was inferior to that of the 7% CdS/g-C_3N_4 composite photocatalyst probably due to the overloading of CdS nanoparticles covering part of the reactive sites, which slightly degraded the degradation performance.

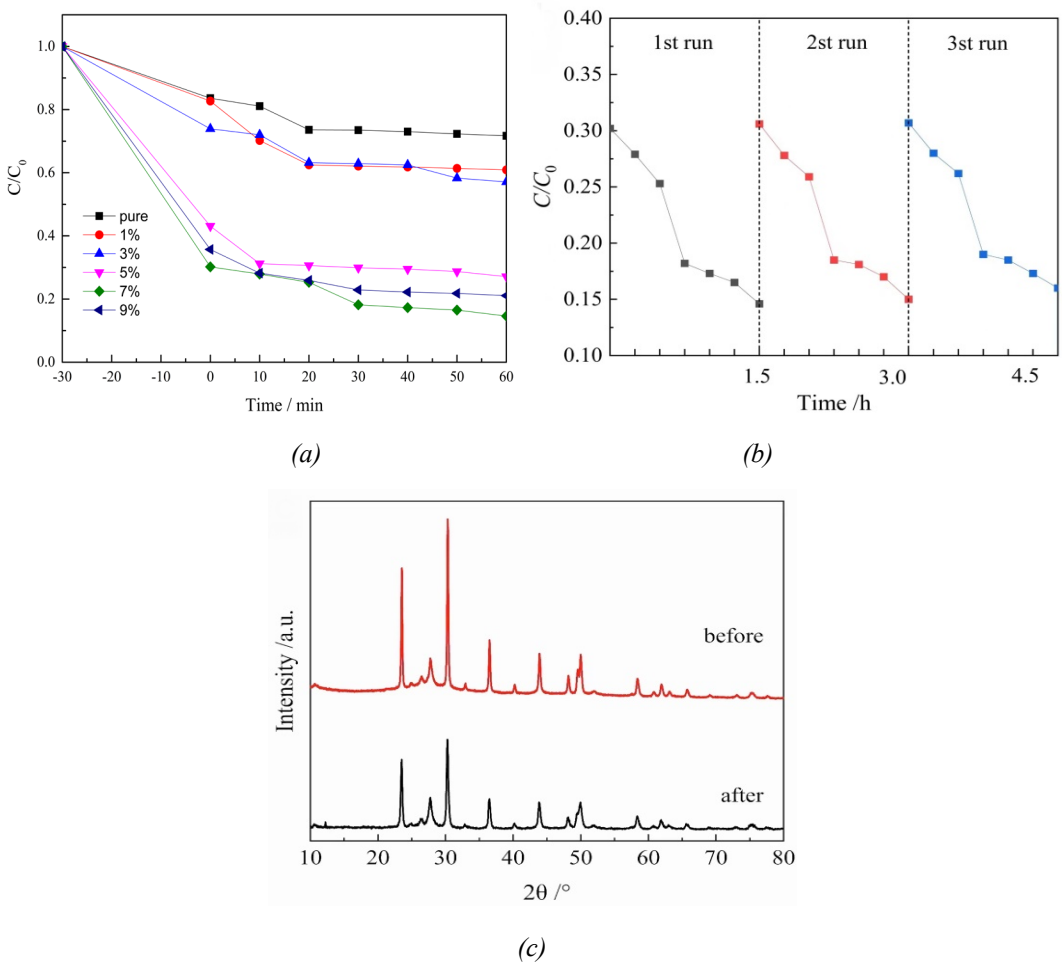

Fig. 7. Photocatalytic degradation of MB with a concentration of 20mg L-1 by photocatalyst(a), cyclic degradation performance test of 7% CdS/g-C_3N_4 photocatalyst(b), XRD patterns before and after 7% CdS/g-C_3N_4 cycle(c).

3.3. Catalytic degradation mechanism

The carrier migration driving force comes from the mutually matching energy band structure between two semiconductors, while the valence band potential of g-C_3N_4 is 1.57 eV and the conduction band potential is -1.12 eV, and the valence band potential of CdS is 1.75 eV and the conduction band potential is -0.39 eV, and their energy band structures just meet the requirements for forming semiconductor heterostructures[29]. Thus, when the composite material receives energy provided by light greater than its band gap energy, electrons on the valence bands of g-C_3N_4 and CdS will jump to their respective conduction bands, and next the electrons on the conduction band of g-C_3N_4 will transfer to the conduction band of CdS, while the holes on the valence band of CdS will transfer to the valence band of g-C_3N_4, which results in the enrichment of photogenerated electrons on CdS and g-C_3N_4

4. Conclusions

Concentrated acid ultrasonic etching and calcination exfoliation were used to break the interlayer hydrogen bonds of g-C_3N_4 nanosheets, and the control of concentrated acid concentration and calcination time was the key to obtain more dispersed and lighter g-C_3N_4 nanosheet structures. Based on this, CdS spherical nanoparticles were loaded on ultrathin g-C_3N_4 nanosheets by hydrothermal method. A series of experimental tests yielded the result that the composite had the highest photocatalytic activity and degraded methylene blue (MB) with an efficiency of 90.7% when the loading mass ratio of CdS on g-C_3N_4 nanosheets reached 7%. What's more, when the composites receive energy provided by light greater than their band gap energy, electrons on the valence bands of g-C_3N_4 and CdS will leap to their respective conduction bands, and subsequently electrons on the conduction band of g-C_3N_4 will be transferred to the conduction band of CdS, while holes on the valence band of CdS will be transferred to the valence band of g-C_3N_4, resulting in the enrichment of photogenerated electrons on CdS and photogenerated holes on g-C_3N_4. This photogenerated electron transfer path within the heterogeneous structure effectively reduces the photogenerated electron-hole pair complexation rate, resulting in a better photocatalytic performance.

Acknowledgements

The authors acknowledge the financial support from Key Natural Science Foundation of Qinghai province (2021-zj-702).

References

[1] T. Takata, K. Domen, ACS Energy Lett. 4(2), 542(2019); https://doi.org/10.1021/acsenergylett.8b02209
[2] T. Wu, P. Wang, J. Qian, Y. Ao, C. Wang, J. Hou, Dalton Trans. 46(40), 13793(2017); https://doi.org/10.1039/C7DT02929B
[3] A. Almohammedia, E. R. Shaabanb, Chalcogenide Lett. 19(10), 701(2022).
[4] Z. Y. Zhang, J. D. Huang, M. Y. Zhang, Q. Yuan, B. Dong, Appl. Catal. B Environ. 163, 298 (2015); https://doi.org/10.1016/j.apcatb.2014.08.013
[5] Z. M. Cuia, C. Z. Dong, Y. L. Lia, Q. J. Zhang, Chalcogenide Lett. 19(3), 197(2022).
[6] D. Qu, J. Liu, X. Miao, M. Han, H. C. Zhang, Z. Cui, S. R. Sun, Z. H. Kang, H. Y. Fan, Z. C. Sun, Appl. Catal. B. 227(5), 418(2018); https://doi.org/10.1016/j.apcatb.2018.01.030
[7] F. Chang, W. J. Ya, W. Cheng, F. Wu, B. Deng, X. Hu, Mater. Sci. Semicond. Process. 87, 1 (2018); https://doi.org/10.1016/j.mssp.2018.07.005
[8] N. Li, Y. Tian, J. H. Zhao, J. Zhang, W. Zuo, L. C. Kong, Chem. Eng. J. 352, 412 (2018); https://doi.org/10.1016/j.cej.2018.07.038
[9] Z. Y. Huang, X. Q. Zeng, K. Li, S. Gao, Q. Y Wang, J. Lu, ACS Appl. Mater. Interfaces. 9(47), 41120(2017); https://doi.org/10.1021/acsami.7b12386
[10] X. M. Liu, Y. Liu, W. K. Zhang, Q. Y. Zhong, X. Y. Ma, Mater Sci Semicond Process. 105, 104734(2020); https://doi.org/10.1016/j.mssp.2019.104734
[11] G. P. Zhang, X. W. Zhu, D. Y. Chen, N. J. Li, Q. F. Xu, H. Li, J. H. He, H. Xu, J. M. Lu, Environ. Sci. Nano. 7(2), 676(2020); https://doi.org/10.1039/C9EN01325C

[12] D. Li, M. Y. Zhu, RSC Adv. 6(31):25670(2016); https://doi.org/10.1039/C5RA27895C
[13] J. C. Wang, J. Ren, H. C. Yao, L. Zhang, J. S. Wang, S. Q. Zang, L. F. Han, Z. J. Li, J. Hazard. Mater. 311,11(2016); https://doi.org/10.1016/j.jhazmat.2016.02.055
[14] Z. L. Fang, H. F. Rong, Z. L. Ya, P. Qi, J. Mater. Sci. 50(8), 3057(2015); https://doi.org/10.1007/s10853-015-8865-8
[15] R. B.Wei, Z. L. Huang, G. H. Gu, Z. Wang, L. X. Zeng, Y. B. Chen, Z. Q. Liu, Appl. Catal. B-Environ. 231, 101(2018); https://doi.org/10.1016/j.apcatb.2018.03.014
[16] J. S. Zhang, M. W. Zhang, L. H. Lin, X. C. Wang, Angew. Chem. Int. Ed. 127 (21), 6395(2015); https://doi.org/10.1002/ange.201501001
[17] H. G. Yu, X. Huang, P. Wang, J. G. Yu, J. Phys. Chem. C. 120(7), 3722(2016); https://doi.org/10.1021/acs.jpcc.6b00126
[18] X. Z. Zhou, J. J. Huang, H. Z. Zhang, H. Sun, W. X.Tu, Int. J. Hydrog. Energy. 41(33),14758(2016); https://doi.org/10.1016/j.ijhydene.2016.06.190
[19] H. G. Yu, W. Zhong, X. Huang, P. Wang, J. G. Yu, ACS Sustain. Chem. Eng. 6(4), 5513(2018); https://doi.org/10.1021/acssuschemeng.8b00398
[20] F. Y. Cheng, Q. J. Xiang, RSC Adv. 6(80), 76269(2016); https://doi.org/10.1039/C6RA16076J
[21] M. Y. Zhang, H. l. Lin, J. Cao, X. M. Guo, S. F. Chen, Chem. Eng. J. 321, 484(2017); https://doi.org/10.1016/j.cej.2017.03.143
[22] K. L. Wu, P. C. Wu, J. F. Zhu, C. Liu, X. J. Dong, J. N. Wu, G. H. Meng, K. B. Xu, J. Hou, Z. Y. Liu, X. H. Guo, Chem. Eng. J. 360, 221(2019); https://doi.org/10.1016/j.cej.2018.11.211
[23] W. L. Yang, X. Xiao, R. X. Lu, H. W. Xie, M. S. Xu, M. Liu, Q. Sun, M. K. Tian, RSC Adv. 6(103), 101242(2016); https://doi.org/10.1039/C6RA11904B
[24] D. Peng, H. Wang, K. Yu, Y. Chang, X. Ma, S. Dong, RSC Adv. 6(81), 77760(2016); https://doi.org/10.1039/C6RA12915C
[25] M. Mousavi, A. Habibi-Yangjeh, Adv Powder Technol. 29(1): 94(2018); https://doi.org/10.1016/j.apt.2017.10.016
[26] C. Ji, C. Du, J. D. Steinkruger, C. Zhou, S. Yang, Mater. Lett. 240, 128(2019); https://doi.org/10.1016/j.matlet.2018.12.128
[27] J. Y. Zhang, Y. H. Wang, J. Jin, J. Zhang, L. Zhang, F. Huang, J. G. Yu, ACS Appl. Mater. Interfaces. 5(20), 10317(2013); https://doi.org/10.1021/am403327g
[28] X. L. Yin, L. L. Li, W. J. Jiang, Y. Zhang, X. Zhang, L. J. Wan, J. S. Hu, ACS Appl. Mater. Interfaces. 8(24), 15258(2016); https://doi.org/10.1021/acsami.6b02687
[29] X. C. Wang, K. Maeda, A. Thomas, K. Takanabe, G. Xin, J. M. Carlsson, K. Domen, M. Antonietti, Nat. Mater. 8, 76(2008); https://doi.org/10.1038/nmat2317